Biomedical Physics & Engineering Express

Endorsed by IPEM Institute of Physics and Engineering in Medicine

PAPER • **OPEN ACCESS**

Investigation of the accuracy of a portable ^{109}Cd XRF system for the measurement of iron in skin

To cite this article: Sami Ullah Bangash *et al* 2024 *Biomed. Phys. Eng. Express* **10** 035032

Biomedical Physics & Engineering Express

PAPER

Investigation of the accuracy of a portable ^{109}Cd XRF system for the measurement of iron in skin

Sami Ullah Bangash[1], **Fiona E McNeill**[1] **and Michael J Farquharson**[2]

[1] Department of Physics and Astronomy, School for Interdisciplinary Sciences, McMaster University, Hamilton, ON, L8S 4K1, Canada
[2] School for Interdisciplinary Sciences, McMaster University, Hamilton, ON, L8S 4K1, Canada

E-mail: bangashs@mcmaster.ca

Keywords: iron, XRF, ICP-MS, synchrotron μXRF, pig skin, minimum detectable limit

OPEN ACCESS

RECEIVED
28 January 2024

REVISED
20 March 2024

ACCEPTED FOR PUBLICATION
11 April 2024

PUBLISHED
22 April 2024

Abstract

We have previously reported the design of a portable ^{109}Cd x-ray fluorescence (XRF) system to measure iron levels in the skin of patients with either iron overload disease, such as thalassemia, or iron deficiency disease, such as anemia. In phantom studies, the system was found to have a detection limit of 1.35 μg Fe per g of tissue for a dose of 1.1 mSv. However, the system must provide accurate as well as precise measurements of iron levels in the skin in order to be suitable for human studies. The accuracy of the system has been explored using several methods. First, the iron concentrations of ten pigskin samples were assessed using both the portable XRF system and ICP-MS, and the results were compared. Overall, it was found that XRF and ICP-MS reported average values for iron in skin that were comparable to within uncertainties. The mean difference between the two methodologies was not significant, 2.5 ± 4.6 μg Fe per g. On this basis, the system could be considered accurate. However, ICP-MS measurements reported a wider range of values than XRF, with two individual samples having ICP-MS results that were significantly elevated ($p < 0.05$) compared to XRF. Synchrotron μXRF maps of iron levels in pigskin were acquired on the BioXAS beam line of the Canadian Light Source. The μXRF maps indicated two important features in the distribution of iron in pigskin. First, there were small areas of high iron concentration in the pigskin samples, that were predominantly located in the dermis and hypodermis at depths greater than 0.5 mm. Monte Carlo modelling using the EGS 5 code determined that if these iron 'hot spots' were located towards the back of the skin at depths greater than 0.5 mm, they would not be observed by XRF, but would be measured by ICP-MS. These results support a hypothesis that iron levels in the two samples that reported significantly elevated ICP-MS results compared to XRF may have had small blood vessels at the back of the skin. Second, the synchrotron μXRF maps also showed a narrow (approximately 100μm thick) layer of elevated iron at the surface of the skin. Monte Carlo models determined that, as expected, the XRF system was most sensitive to these skin layers. However, the simulations found that the XRF system, when calibrated against homogenous water-based phantoms, was found to accurately measure average iron levels in the skin of normal pigs despite the greater sensitivity to the surface layer. The Monte Carlo results further indicated that with highly elevated skin surface iron levels, the XRF system would not provide a good estimate of average skin iron levels. The XRF estimate could, with correction factors, provide a good estimate of the iron levels in the surface layers of skin. There is limited data on iron distribution in skin, especially under conditions of disease. If iron levels are elevated at the skin surface by diseases including thalassemia and hemochromatosis, this XRF device may prove to be an accurate clinical tool. However, further data are required on skin iron distributions in healthy and iron overload disease before this system can be verified to provide accurate measurements.

Introduction

Iron overload and skin iron storage

We have previously described the development of a portable x-ray fluorescence system for the *in vivo* measurement of iron in the skin [1]. The system was designed to measure the potentially elevated iron levels in the skin of patients suffering from hemochromatosis or thalassemia [2]. The liver is the primary storage site and a target organ for excess iron in the body, with excess iron in the liver causing cirrhosis, hepatic fibrosis and carcinoma [3]. However, it is difficult to measure the liver. Studies have shown a strong correlation between skin iron and liver iron concentrations [2, 4], and so a measure of iron levels in the skin by XRF is intended as a surrogate measurement for iron overload in the liver (and potentially other organs).

The system is fully described in our previous work [1]. However, to summarise: the silver x-rays from the electron capture decay of ^{109}Cd to ^{109}Ag are used as a fluorescing source to excite iron atoms in skin samples as shown in figure 1). The source is combined with a silicon drift detector to detect the characteristic x-rays from iron in the sample in an approximate 180° backscatter geometry as shown in figure 1. The system was calibrated against water-based iron phantoms and achieved a phantom-based minimum detectable limit (MDL) of 1.35 μg Fe per g in a 30-minute (real-time) measurement delivering a dose of 1.1 mSv to the skin.

The precision of the system in phantom measurements is thus well known. However, before the system can be used for *in vivo* measurements, it is necessary to test whether XRF measurements of the iron levels in the skin are accurate. In addition, we wanted to know whether our phantoms can be considered a good calibration model for skin and whether the MDLs of an *in vitro* skin model differ from the MDL in phantoms. Our system is calibrated using homogenous water phantoms, but the structure of skin is more complicated. Skin consists of two main layers, the epidermis and dermis. The epidermis is the skin's outermost layer and is further divided into five layers. The stratum basale lies deep and close to the dermis; the stratum spinosum, the stratum granulosum, and stratum lucidum are present in thick skin like palms and soles, and the stratum corneum, which is the outermost layer of skin. The deep skin layer, the dermis, contains blood vessels and nerve endings [5].

The depth distribution of iron and the presence of blood vessels in the skin may complicate the measurement of iron by XRF. The distribution of iron is still not well known: one study of cadaver samples showed that the maximum iron content was found in the deep layer of the epidermis, the stratum basale; a further study of iron levels in patients with haemachromatosis indicated raised iron levels in the stratum corneum and epidermis during different phases of the disease [6, 7].

The XRF system does not detect iron in the different layers of skin equally well. The sensitivity of the system, i.e., the detected number of iron counts per mg of iron, falls with increasing depth, and iron at sites deeper than 0.5–1 mm is not detected. It is not known if the XRF measurement of iron can be considered an accurate measurement of the 'bulk' sample in real skin. Hence, it is essential to test the XRF instrument's performance and accuracy prior to clinical application.

This article describes work that is the first step in assessing whether the ^{109}Cd-based portable XRF system can accurately measure iron levels in skin, and whether homogenous water-based phantoms can be considered a good calibration model for XRF measurements of iron in skin. We compare the measurement precision of phantoms and skin and describe validation studies performed to compare XRF analysis of pigskin iron concentrations against the total iron content of the same samples measured with Inductively Coupled Plasma Mass Spectroscopy (ICP-MS). We provide new information on iron distribution in pigskin assessed using synchrotron μXRF, and show, through the use of Monte Carlo models of varying skin iron concentration, the factors which may impact the accuracy of the XRF measurement system.

Methods and materials

Pigskin as a model for human skin measurement

Human skin is generally not very readily available and requires human research ethical approval prior to use. In addition, the Public Health Agency of Canada recommends that work with human samples be performed to biosafety level 2 standards. In the current study, iron concentrations were therefore measured in ethically sourced pigskin due to the similarities of pigskin with human skin [8]. Pigskin is composed of an epidermis and dermis, similar to human skin, and the ratios of their epidermis thickness are comparable [9, 10]. Numerous studies have used pigskin as a substitute for human skin [8, 9, 11] and so the substitution of pigskin for human skin was considered acceptable for system validation.

As this work did not involve live animals, ethical approval from an animal research ethics board was not required for the study. Fresh skin of domestic pigs was sourced from a local butcher. This is considered ethical sourcing as the skin was marked for disposal. The pigskin was thus food grade, and this work did not require biosafety approval, although samples were disposed of into the biohazard waste stream after use.

Portable XRF and ICP-MS Comparison

Our *a priori* expectation of the comparison of iron levels as measured by ICP-MS and XRF was that the two techniques would measure the same iron concentrations if a) the two techniques measured the identical

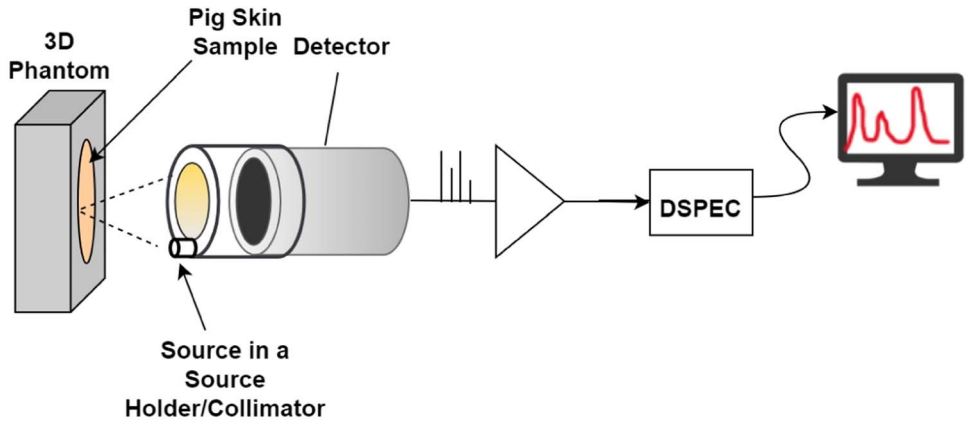

Figure 1. Experimental setup for measuring pigskin concentration. The skin sample is mounted at 0.5 cm from the source [1].

surface areas of the same samples and b) iron in the pigskin could be considered to be relatively homogeneously distributed. The techniques might not match if the iron had a strong spatial distribution with depth through the skin.

This assumption was made because the two techniques sample slightly different volumes. The working principle behind XRF analysis is the photoelectric effect. Silver photons from our ^{109}Cd radioactive source can create a vacancy in an iron atom in the sample when an inner shell electron absorbs the photon energy and is emitted from the atom. The electronic transitions from the higher shells to the lower shells to fill the vacancies can result in x-rays being emitted, the energy of which is the difference in the energy of the transition shells involved. The x-rays are characteristic of and specific to iron and are then measured with a suitable detector. The ^{109}Cd silver x-rays that are used as the fluorescing source in this system are 22 and 25 keV, while the characteristic Kα_1 x-rays from iron are of energy 6.4 keV. These silver and iron x-rays are highly attenuated by soft tissue. The intensity of an iron signal received at the detector from a sample in our XRF measurement is a strong function of depth. To a first approximation, the drop off in iron signal with depth depends on the attenuation of the silver x-rays as they enter the tissue multiplied by the attenuation of the iron x-rays as they exit the tissue. There are additional geometric factors as the angle subtended by the detector from a point in the sample varies with depth. The XRF measurement, therefore, does not sample equally through the depth of the tissue. A higher proportion of the overall XRF signal comes from volumes near the surface of the skin sample than volumes further back.

XRF measurements were compared to analysis of iron content of the same samples by inductively coupled plasma mass spectroscopy, because it is a relatively standard technique for the elemental analysis of biological and environmental samples [12]. ICP-MS has many advantages for measuring elemental concentrations in a sample: high sensitivity and low

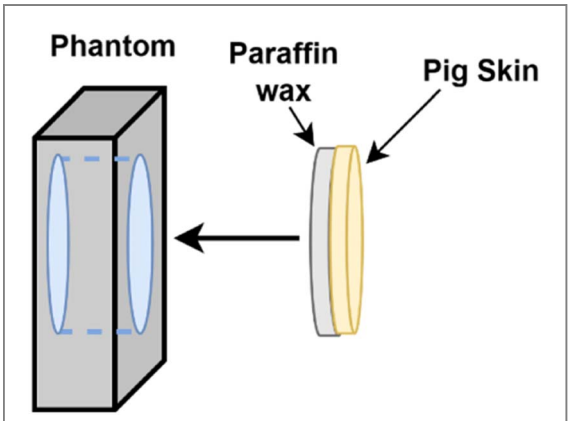

Figure 2. The phantom is filled with pigskin sample, with paraffin wax positioned behind the skin to replicate similar scattering properties to those of tissues. Reproduced from [1]. CC BY 4.0.

detection limits for most elements down to parts per billion (ppb) levels [13]. The limitation of ICP-MS as a comparison to XRF is that it measures the average concentration of iron over a bulk sample, as tissue samples are homogenized and digested in acid prior to measurement.

Pigskin sample preparation

The whole skin layer plus the underlying layer of subcutaneous fat, was cut and included in the measurement. The pigskin samples consisted of both the skin and the subcutaneous fat behind the skin and were approximately 5 mm deep, with the skin layer being approximately 2 mm thick. The volume of the phantom behind the skin was filled with paraffin wax before inserting the skin samples (figure 2).

Paraffin wax is composed of carbon and hydrogen and has x-ray scattering properties similar to human (and pig) soft tissue. Ten samples of fresh pigskin, each a 4 cm diameter circle cut to fit into the front phantom face, were cut and stored in the freezer prior to measurement. The ten samples were cut from two larger sheets of pigskin. It was not known if the two pigskin sheets came from one or two pigs.

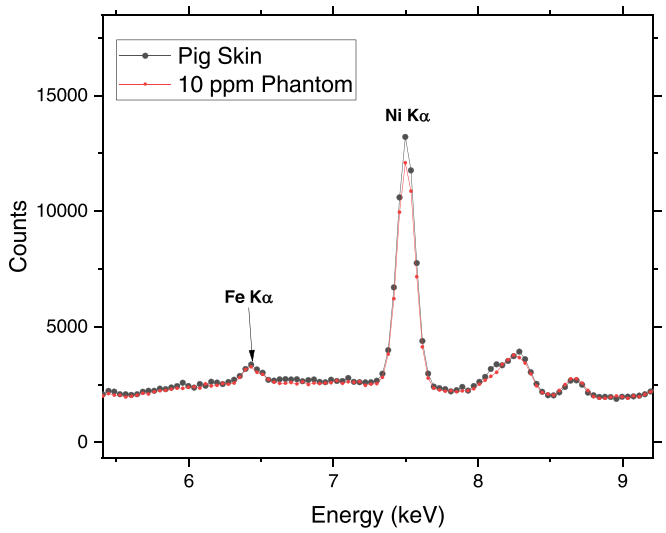

Figure 3. A comparison of a pigskin XRF spectrum and a 10 ppm water-based calibration phantom. The phantom and skin spectra display the similar spectral features and are of a similar intensity.

Portable system pigskin experiment

The XRF system details have been fully described previously in other work, but we provide some information here to explain the pigskin measurements. A ^{109}Cd source was used to irradiate the 4 cm diameter skin samples that had been inserted into the front-face of the phantoms as shown in figure 2. The source is in a tantalum collimator, attached to one side of the detector onto a styrene window, as shown in figure 2. The collimator ensures that the detector cannot see direct emissions from the source. The system is said to be in a 180° or backscatter geometry. The source activity at the time of measurement was 0.109 GBq.

Iron characteristic x-rays produce a signal in the detector and, after amplification, are processed by an Ortec Digital Gamma-Ray Spectrometer (DSPEC). The acquisition of the data is carried out with Gamma Vision software. The dead time during measurement was low, approximately 5%. The samples were measured for a live time of 1800 s, and each measurement was repeated three times to get a better estimate of the uncertainty in a measurement.

The source is collimated and so only irradiates a small surface area of skin. To compare the XRF and ICP-MS samples, it was important to ensure both techniques measured the same skin sample areas. The skin samples were cut to 4 cm in diameter to fit in the phantom but were cut down further, to the beam sample area, before being sent for analysis by ICP-MS. The area irradiated by the ^{109}Cd source on the larger 4 cm diameter skin samples was estimated using chromatograph films. As the irradiation area at the sample surface is dependent on the distance between the sample and the source, the same geometry was used for beam size measurement and XRF measurements on the skin samples. A circular dark spot of 1 cm diameter appeared on the chromatograph film after exposure to the x- and γ-rays from ^{109}Cd and the darkened spot on the film permitted identification of the measurement area.

After the XRF measurements the circular surface area of 1 cm diameter that matched the measured irradiation area was cut from the skin samples, and the subcutaneous fat layer underneath the skin was removed, before sending the samples to the Analytical and Environmental Services Laboratory of Kinectrics Canada to measure total iron content by ICP-MS.

A typical spectrum resulting in the skin measurement is shown in figure 3. The prominent peak from nickel Kα x-rays in the spectrum is due to the presence of nickel in the detector. This nickel peak is used to normalize the measurement system, which allows for a more robust XRF measurement. We have shown that the ratio of Fe x-ray signal to Ni x-ray signal does not change with distance from the detector [1].

μXRF Measurements of iron distribution in skin

A μXRF image of iron distribution in pigskin was made available from a separate ongoing study in our laboratory. That study is of percutaneous absorption of Pb in pigskin (CLS project number 37G12956). However, pigskin samples from the same source as previously described for portable XRF and ICP-MS measurements, were measured as blank standards as part of that study. The samples were trimmed and had the subcutaneous layer of fat removed. They were not exposed to lead, instead samples had 100 μl of phosphate buffered saline placed on the skin surface and left to diffuse into the skin for 24 h. After saline diffusion, the samples were freeze microtomed to 25 μm thick sections and placed onto 4 μm thick XRF film microscope slides. The sample was XRF scanned at 20 μm resolution using the Bio-XAS beam line of the Canadian Light Source with an excitation energy of 13.45 keV. The iron signals were extracted from each

measurement pixel using the PyMCA code and a 2-dimensional map of the relative iron level in the skin was obtained.

Monte Carlo simulations

The effects of variations in iron distribution that differed from the *a priori* assumption that iron in pigskin was homogeneously distributed in pigskin were not known. Monte Carlo simulations of the system were performed to test the effects of iron distribution on XRF measurement. The XRF system was simulated using the Electron Gamma Shower version 5 (EGS5) Monte Carlo code. This is a well developed code frequently used for x-ray studies, that permits the coupled transport of electrons, positrons and photons within a given geometry. The simulation modelled the experimental system geometry illustrated in figure 2. The model incorporated the detector geometry, comprised of the Si detector with an aluminum cap and a tantalum source collimator, as utilized for the XRF analysis of pigskin iron. The x-ray excitation energies were set to those of the silver x-rays (22.1 keV and 24.9 keV) and the 88 keV gamma rays from the source were also incorporated into the model.

The model performance was first tested against the experimental calibration of the portable XRF instrument to assess the accuracy of the simulation. The experimental system uses a normalized calibration line of Fe Kα x-ray peak area to the Ni Kα x-ray peak area. Ideally, the experimental and modelled system comparisons would have been of this ratio. However, in this instance, the full details of the experimental system were not known. The detector manufacturer considers certain information proprietary, and the information is not disclosed. For example, the experimental system utilizes a nickel x-ray signal from the detector for normalization to compensate for both the variations in phantom-to-detector distance and the radioactive decay of the source. However, the exact location, mass etc. of the nickel in the system is uncertain. Attempts were made to simulate the presence of the nickel in the detector setup, but an exact match between experiment and model could not be obtained without the knowledge of the location, mass and distribution of the nickel. Instead, the simulated model was verified by showing that experiment and simulation Fe K_α counts were correlated for a fixed geometry, and the simulation could thus be used to predict measurement system results.

The experimental calibration of the portable XRF instrument was based on water-based phantoms and so water-based phantoms of volume 25 ml with varying iron concentrations were simulated using the EGS5 code, and a calibration line was developed from simulated data. The validated Monte Carlo model was then used to simulate distributions of iron that were indicated from synchrotron μ-XRF measurements of iron in pigskin. These included simulations of hot-spots created by blood vessels in the skin, and heterogeneous distributions of iron across the skin layers.

Results

Pigskin and phantom spectral comparison

The XRF spectrum obtained from one of the pigskin samples is shown in figure 3. A phantom spectrum is shown in the same chart for comparison. As can be seen, the phantom and the skin sample have approximately the same spectral shape and background. The average uncertainty in repeat measurements of a 10 ppm calibration phantom and the pigskin samples was found to be similar: 12.7 ± 0.6 μg Fe per g and 11.3 ± 1.8 μg Fe per g, respectively. Thus, the water-based phantom appears from spectral examination, and comparison of measurement reproducibility, to be a relatively good model for XRF measurements of skin. It also has the benefits of being low-cost and simple to create.

Our previous published work on this system found a detection limit in phantoms of 1.35 ± 0.35 μg Fe per g in a 30-minute (real-time) measurement. The phantom detection limit at the time of this work was found to be slightly higher, but not significantly so: 1.48 ± 0.99 μg Fe per g. A small increase was expected due to the decay of the radioactive source since the previous set of published data.

Comparison of iron analysis by XRF and ICP-MS

The comparison of the results from the portable XRF system and the reported concentrations from ICP-MS measurements for the 10 pigskin samples is summarized in table 1.

The Poisson statistics which govern XRF measurements mean that if the estimates by XRF and ICP-MS were equal on average, we would expect in five cases the XRF estimate would be higher than the ICP-MS estimate and vice versa. As can be seen in table 1, the XRF results are similar to ICP-MS results, with seven samples where the ICP-MS estimate is higher than the XRF estimate. However, the difference in estimate between the ICP-MS estimate and the XRF estimate is significant at the 95% confidence level in only two samples; S2 and S6 (shaded grey in the table). The differences between the individual sample estimate from XRF and ICP-MS vary from-14.7% to 44.1% (-1.6 to 8.9 μg Fe per g), with the ICP-MS estimates being on average 13.4% (2.5 μg Fe per g) higher than the XRF estimates, suggestive of a trend towards higher ICP-MS than XRF estimates.

The iron concentration distributions of the two data sets from XRF and ICP-MS are shown in figure 4. Anderson-Darling normality tests were applied (using Minitab) to the two distributions; XRF estimates and ICP-MS estimates. Given the limited number of

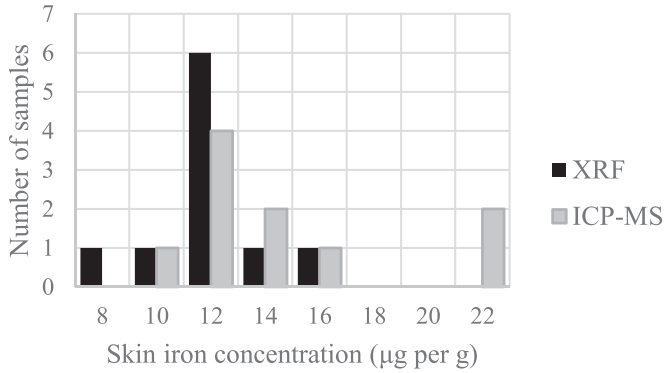

Figure 4. The distributions of skin iron levels measured by XRF and ICP-MS.

Table 1. Results in μg Fe per g of XRF and ICP-MS analysis of pigskin samples. XRF results are reported as the average of three measurements, and the XRF uncertainty is reported as the standard error of the mean. ICP-MS results were not reported with uncertainty but were quoted as having a detection limit of 1 μg Fe per g, from which it is inferred that each sample should be considered to have a measurement uncertainty of 0.3–0.5 μg Fe per g. The two samples in the table marked in dark grey are the two samples where the ICP-MS and XRF measurements are significantly different from each other.

Sample	XRF Mean Estimate	XRF Standard Error	ICP-MS Estimate	% Difference
S1	11.7	6	10.2	−14.7
S2	13	3	20.9	37.7
S3	14.2	5.1	12.6	−12.7
S4	9.3	5.3	10.4	10.6
S5	11.4	4.4	15.5	26.5
S6	11.3	4.7	20.2	44.1
S7	7.7	3.4	8.8	12.6
S8	10.8	4.3	10.2	−5.9
S9	10.1	5.1	13	22.3
S10	10.4	4.8	12	9.6

Table 2. Paired t-test analysis for XRF and ICP-MS data.

	XRF	ICP-MS
Distribution Mean (μg Fe per g)	11.0	13.48
Variance	3.3	17.8
t Stat	−2.06	
P(T<=t) one-tail	0.035	
P(T<=t) two-tail	0.070	

samples, the test was set to reject the normality hypothesis if the p-value was less than 0.05.

It was found that both the ICP-MS ($p = 0.068$) and XRF data ($p = 0.892$) could be considered normally distributed. Paired t-tests were applied to determine whether the mean of the ICP-MS and the mean of the XRF data are the same, i.e., whether on average, the two sets of skin iron estimates are comparable. The results of the paired t-test are shown in table 2.

The paired t-test result found that a mean XRF estimate of the XRF measurements of 11.0 ± 1.8 μg Fe per g compared to a mean ICP-MS estimate of 13.5 ± 4.2 μg Fe per g ($p = 0.034$, one-tailed test and $p = 0.068$, two tailed test). The one-tailed paired t-test is significant at the 5% level, which would suggest that the mean ICP-MS estimate of iron in the pigskin samples is higher than the XRF estimate. However, there was no prior expectation that ICP-MS estimates would always be higher, so a one-tailed test is possibly unfair. The two-tailed t-test indicates that the two sample means are not different at the $p = 0.05$ level. In this small sample, the XRF can be considered, on average, to accurately assess iron levels at a 95% confidence interval level in the skin as estimated by ICP-MS. However, while the one-tailed paired t-test is not fair given prior expectations, it, and the individual sample differences shown in table 1, may suggest a pattern to the data. As shown in figure 4, the two samples that were measured as having a significantly different iron content by ICP-MS compared to XRF are both much higher than the XRF result.

There was no evidence of a pattern to the data when a linear regression analysis was performed of the XRF estimates against the ICP-MS estimates, $p = 0.14$. However, when a linear regression was performed of the difference between the ICP-MS values and XRF values against the ICP-MS values, it was found to be highly significant, $p = 0.0004$. This regression is plotted in figure 5. The graph shows that the difference between the XRF and ICP-MS values increases with increasing ICP-MS value. When the difference between the XRF estimate and the ICP-MS estimate was regressed against the XRF estimate, the relationship was found to not be significant, $p = 0.83$.

Overall, the data show that the ICP-MS estimates show more variation and a wider range of iron concentration values than the XRF estimates, and the difference between estimates is dependent on the ICP-MS measurements. The ICP-MS estimates trend

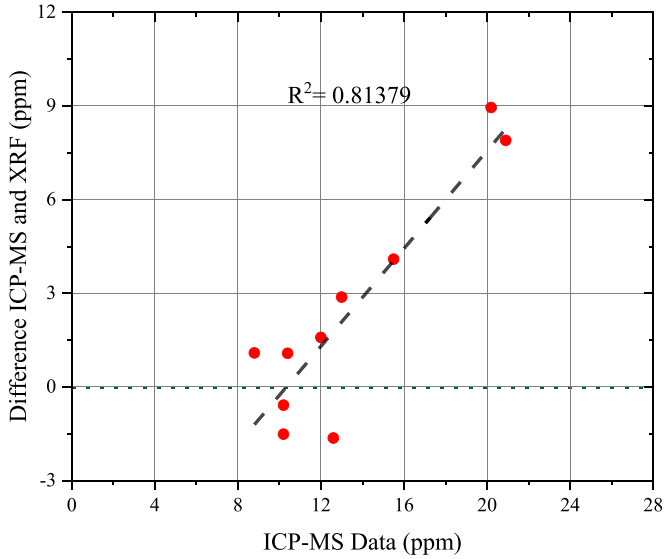

Figure 5. A plot of the difference in concentration as assessed by ICP-MS and XRF versus ICP-MS.

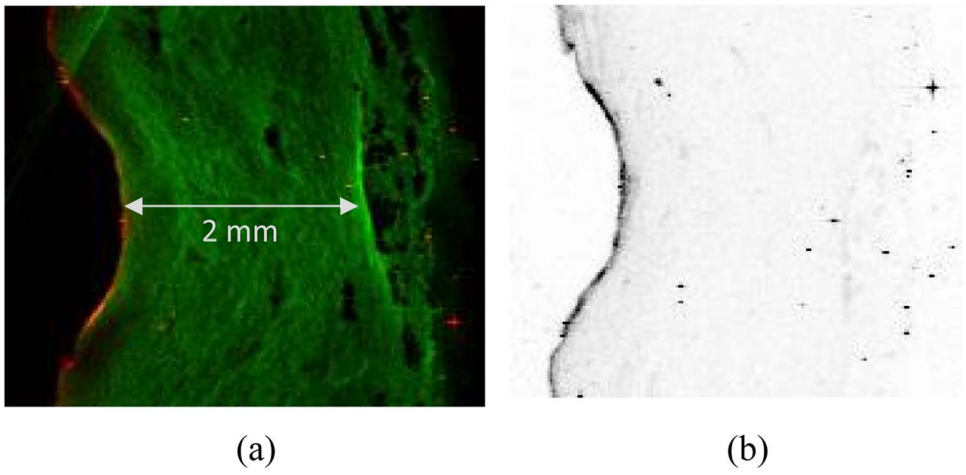

Figure 6. The distribution of iron in pigskin as assessed by synchrotron μXRF. These are two images of the same sample measurement. The skin surface, the stratum corneum, is on the left in each image. The resolution of both these images is 20 μm per pixel. The colour image (a) shows the distribution of Fe in red, and the distribution of chlorine in green to orient image (b) against the position in skin. The black and white image (b) is of the iron distribution only.

towards higher values than the XRF estimates. This may suggest that there may be iron in specific skin samples that is measured by ICP-MS but is not measured by XRF because of the decreasing sensitivity of the XRF measurement with depth.

μXRF maps of iron in skin

The possibility of areas of increased iron towards the back of the sample is confirmed by the synchrotron μXRF image (figure 6). It can be seen that there are iron 'hot spots' at points in the sample that possibly relate to microvasculature in the skin. The number of observed hot spots increases with depth in this sample with more hot spots located in the dermis and hypodermis. In this sample, there is one observable hotspot at a depth of 260 μm below the skin surface; four hot spots at depths between 500 and 800 μm; and twelve hot spots at depths greater than 1500 μm. Figure 6 also suggests that iron is not homogenously distributed but more concentrated at the skin surface. The synchrotron μXRF data suggest a layer of higher iron level of approximate thickness 100 μm at the surface of the skin.

Simulation results

The initial Monte Carlo simulations modelled measurement of homogeneously distributed water-based iron-doped phantoms. The simulated iron Kα x-ray signals for specific concentrations were strongly correlated with the experimental iron K_α x-ray signals, $p < 0.0001$ and $R^2 = 0.946$. The slope of the regression was 1.13 $\pm$0.12, so the peak area per unit

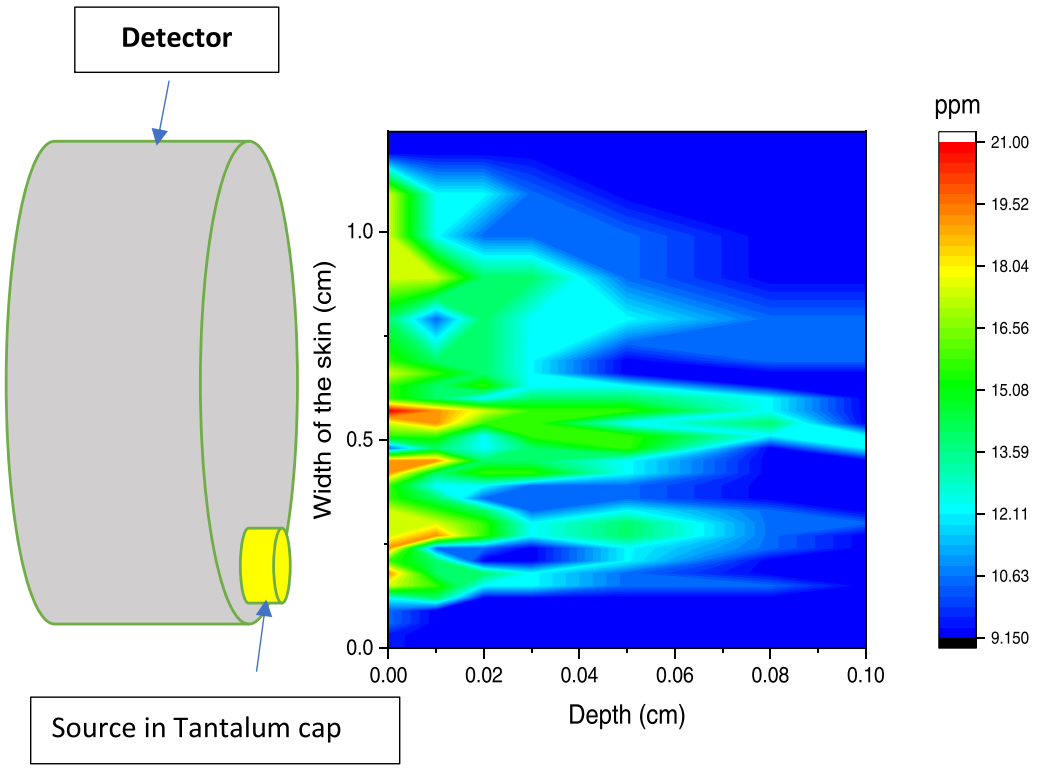

Figure 7. 2D contour plot representing the effect of iron hot spots on an XRF measurement at various locations in the skin.

concentrations were found to be the same to with uncertainties. The experimentally measured iron concentration in non-homogeneous phantoms should be predictable from the simulation as long as the experimental geometry remains fixed.

Using the verified EGS 5 model, simulations were performed to investigate whether remnants of blood vessels (presumed to be the source of iron 'hot spots') at various skin depths could produce the results that would explain observed differences in the pigskin iron levels measured by XRF and ICP-MS. The presence of small blood vessels were modelled using a circular cylinder of thickness of 0.2 cm and diameter 2 cm with a total mass of 0.6284 g to represent the skin. Pigskin samples were previously found, on average, to contain approximately 11 ppm of iron, and so the concentration of iron in the cylinder was set to this value. In comparison, whole blood has an average iron content of 50.3 mg Fe per dL which approximately equivalent to 500 ppm [14]. Small spheres of diameter 0.29 cm filled with tissue with Fe concentrations of 500 ppm were therefore modelled at various points through the skin to determine the locations where hot spots would be measurable in a portable XRF measurement. Hot spots would of course be measured in all locations in a hypothetical ICP-MS measurement of the same sample.

Figure 7 illustrates a 2D contour plot showing the impact of an Fe hot spot at various positions within the skin. The x-axis denotes the depth into the skin, while the y-axis represents the width (i.e. the position on a line across the diameter) of the circular face of the skin. Changes in the measured iron level are shown on a colour scale. Blue indicates no change in measured signal, while red indicates a large change in measured signal. It can be seen that XRF will likely not detect residual blood vessels beyond a skin depth of 0.5 mm. In addition, there are locations off-axis from the source where blood vessels closer to the surface than 0.5 mm remain undetected. The maximum effect of the presence of small blood vessels on the portable XRF measurement is when the vessels are near the skin surface. While the synchrotron μXRF map shown in figure 6 has seventeen observable iron hotspots, only one hot spot would be detectable by the XRF system, as sixteen of the hotspots are at depths greater than 0.5 mm. This data therefore aligns with the hypothesis that dependant on location, small fragments of blood vessels, e.g., not removed with the fat at the back of the skin or small vessels within the skin, would be detectable by ICP-MS but not by XRF.

In addition to hot spots, the synchrotron images suggest a high iron layer at the skin surface. A Monte Carlo simulation was performed to model the effect of a 100 μm thick high iron layer at the front of the skin. The skin behind this layer was modelled by a lower iron concentration. The goal of this simulation was to investigate the impact of an inhomogeneous distribution of iron within the skin on the XRF signal, and the accuracy of measurement if this XRF signal was used to estimate skin iron level using homogenous phantoms. Various iron concentrations in the front layer were simulated, while keeping the concentration in the back layer constant at 11 ppm.

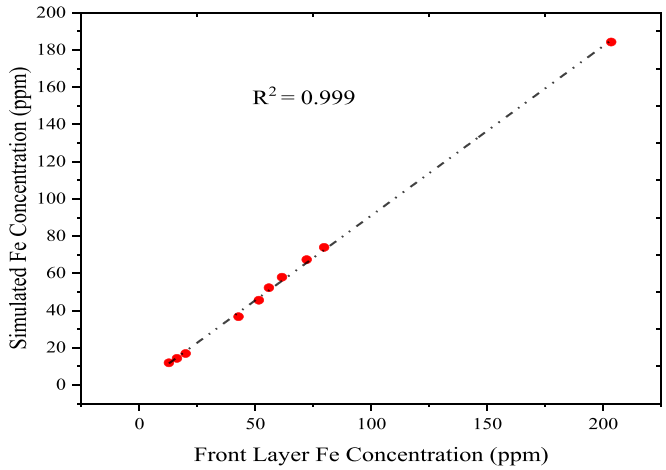

Figure 8. The observed correlation between the iron concentration estimated by XRF and the front iron layer concentration as simulated using the Monte Carlo code EGS 5.

Table 3. Results of the simulation comparing surface layer iron concentration, average iron concentration and XRF estimate of iron concentration The high iron layer at the skin surface is assumed to be 100 μm thick and the back layer is assumed to have a concentration of 11 ppm. At low surface iron concentrations, the XRF and ICP-MS are predicted to produce estimates that are the same to within experimental measurement uncertainties.

Front layer Fe content (ppm)	Average Fe content (ppm)	Simulated XRF estimate of Fe content (ppm)
12.8	12.2	11.9
16.3	13.4	14.3
20.0	14.0	16.9
42.8	19.7	36.7
51.5	21.9	45.5
55.9	23.0	52.2
61.5	24.4	57.9
72.2	27.0	67.3
79.7	34.6	74.0
203.5	75.8	184.3

Table 3 provides a comparison between the average iron concentration that would be hypothetically measured by ICP-MS and the XRF estimated iron concentration using homogeneous phantoms for calibration.

The results presented in table 3 demonstrate that the XRF primarily detects the iron in the front layer. This observation highlights the higher sensitivity of the portable XRF system towards the front layer in comparison to ICP-MS, which quantifies the average iron concentration across the entire skin sample.

Figure 8 shows the iron concentration of front layer plotted against the XRF estimate of iron concentration as calculated from the simulation.

Discussion

XRF measurements in pigskin samples sample a thinner layer of the skin than ICP-MS measurements. The portable XRF system probes approximately the first 0.5 mm of skin, while the ICP-MS analysis measures the whole 2 mm depth. Despite this difference, XRF and ICP-MS analyses of iron levels in skin were found to be the same on average to within 95% confidence levels in 10 pigskin samples. However, in two individual samples, the ICP-MS estimates of iron content were significantly higher than the XRF estimate, and over the 10 samples the ICP-MS measurements identified a wider variation in iron content in the skin samples than XRF measurements, with 70% of samples having estimates of iron that were higher measured by ICP-MS than measured by XRF. Synchrotron μXRF measurements of iron distribution in skin and Monte Carlo simulations support the hypothesis that the higher iron content measured by ICP-MS is likely due to iron deposits (possibly from blood vessels) deeper in the skin. In the synchrotron μXRF map shown in figure 6, sixteen of the seventeen 'hot spots' would not be measured by XRF, but would be measurable by ICP-MS. The iron distribution in lead-dosed pigskin samples from CLS project number 37G12956 showed similar distributions of iron in skin to the blank sample presented here. Most iron 'hot spots' were observed at depths greater than 0.5 mm so would be measured by ICP-MS only, but the occasional hot spot was observed nearer the surface that would lead to an increase in the measured XRF signal.

In this study, skin samples were cut down from the skin surface to the bottom of the dermis, and there may have been small amounts of subcutaneous tissue, containing vascular and capillary tissue, left on the back of the sample. The ICP-MS measurements may therefore not be estimates of iron content in skin only. However, μXRF measurements of iron distribution in skin do suggest the possibility of small blood vessels within the epidermis and dermis. As previously stated, these would be measured by ICP-MS at all depths, but

only by XRF if they are located near the surface of the skin.

The synchrotron μXRF map of iron distribution in pigskin suggests not only that there are hot spots in skin, but that there is a layer of higher iron concentration at the surface of skin. This result is different than observed in prior studies of human cadaver data, where the highest iron concentrations were at the epidermal/dermal boundary. However, in another biopsy sampling studies of people suffering from hemochromatosis, a similar pattern of elevated iron in the stratum corneum and outer layers of skin was observed in certain stages of the disease [6, 7].

The observation of a high iron surface layer in μXRF measurements led to Monte Carlo analysis of this skin surface iron distribution. The XRF system is more sensitive to this surface iron layer. However, the simulations determined that the XRF system would accurately measure average iron levels in normal pigs when calibrated against aqueous phantoms despite this increased sensitivity. This prediction matches the experimental data where 80% of samples had XRF and ICP-MS estimates that were within uncertainties of each other. However, if the iron level increases substantially in the front layer, then at high iron levels, the ICP-MS and XRF estimates are expected to diverge. the Monte Carlo models predicted a strong correlation between iron concentration in the front layer of the skin and the estimated iron concentration measured by the portable XRF system, $R^2 = 0.99$ and $p < 0.0001$. The slope of the relationship is 0.91 ± 0.01. The relationship is not 1:1 which suggests that while the XRF estimate is dominated by the signal from the front iron layer, there is a contribution to the XRF estimate from the lower concentration tissues further back in the skin. The XRF estimate is therefore not accurate at solely determining the iron content of the front layer, nor is it completely accurate compared to ICP-MS in estimating the average iron content over a 2 mm depth of skin. However, if the iron layer is of a relatively constant thickness in all skin samples, then this relationship suggests that applying a correction factor to the XRF estimate could result in an accurate estimate of the level of iron in the surface layer. If correction factors are possible, then the current homogeneous water-based calibration phantoms could be used. This would make phantom construction simple as they are readily manufactured, reproducible and straightforward to measure. They can be made quickly and are low-cost.

The application of a correction factor depends on verification of this distribution of iron in skin. The evidence is relatively scant. Three studies have investigated the distribution of iron in human skin under conditions of iron overload, such as hemochromatosis [15–17]. These investigations highlighted elevated iron concentrations across various layers of the skin. Particularly heightened iron levels were observed in the stratum basale, the deepest layer of the epidermis, although increased iron concentrations were also detected in upper layers of the epidermis. Overall, the human epidermis has a thickness ranging from 76.9 ± 26.2 to 267.4 ± 120.6 μm [18]. Any significant elevated iron layer in the epidermis should be detectable by XRF even in deepest epidermal layers. However, the consistency of the thickness or position of a high iron layer in conditions of iron overload remains uncertain. If position or thickness are found to be variable, additional methods, perhaps using differential attenuation techniques, would be required to establish the iron distribution in an individual before this XRF system could be used. Development of such technology would be a significant undertaking. Further studies are thus required of iron distribution is skin e.g., μXRF synchrotron measurements on human skin samples in iron overload conditions to verify iron distributions in order to fully assess the accuracy of this portable XRF system *in vivo*.

Even if the finding of an elevated surface iron distribution is validated, there are yet further studies must be performed with this system. While previous studies have determined that increases in iron level in skin can be observed under conditions of iron overload, this portable XRF system has never been tested under those conditions. Studies must be performed using this XRF system on skin from iron overload studies to determine the system's ability to distinguish between 'normal' and overloaded groups or individuals.

Conclusion

The accuracy of a hand-held XRF measurement was tested using XRF measurements of healthy pigskin, which were analyzed by ICP-MS. The system performed well, with the mean difference between XRF and ICP-MS being 2.5 ± 4.6 μg Fe per g. Two individual samples had ICP-MS estimates that were significantly higher than XRF estimates. Synchrotron μXRF maps of iron in skin and Monte Carlo models are consistent with a hypothesis that small blood vessels towards the back of the skin can be observed by ICP-MS but not portable XRF. Furthermore, μXRF mapping suggests that iron may be increased in a narrow layer at the surface of the skin. Monte Carlo models predict that if iron is higher at the skin surface then the portable XRF estimate will reflect the raised iron levels at the surface and may be a clinically useful measurement. However, further studies of iron distribution in skin are required to verify this distribution of iron.

Acknowledgments

The Government of Canada's NSERC Discovery program and the Higher Education Commission Pakistan provided funding for this research.

μXRF measurements were performed at the Bio-XAS beam line of the Canadian Light Source. The authors are very grateful to Dr Gosia Korbas and Dr Ibi Bondici for their advice and help with our work on this beamline.

The authors thank Dr Bruce Wainman of the Department of Pathology and Molecular Medicine, McMaster University and Dr Michelle Zeller of the Division of Hematology & Thromboembolism, Department of Medicine, McMaster University, for their ongoing support of this project. Their advice on iron distribution, skin structure, iron overload disease and the implementation of devices in clinical environments has been invaluable in the development of this device.

Data availability statement

All data that support the findings of this study are included within the article (and any supplementary files).

ORCID iDs

Sami Ullah Bangash https://orcid.org/0000-0003-3229-857X

References

[1] Bangash S U K, McNeill F E, Farquharson M J and Chettle D R 2022 Feasibility of a 109Cd-based portable XRF device for measuring skin iron concentration in anaemic and β −Thalassaemic patients *Biomed. Phys. Eng. Express* **8** 065034

[2] Farquharson M J, Bagshaw A P, Porter J B and Abeysinghe R D 2000 The use of skin Fe levels as a surrogate marker for organ Felevels, to monitor treatment in cases of iron overload *Phys. Med. Biol.* **45** 1387

[3] Barton J C 2010 *Handbook of iron overload disorders* (Cambridge University Press) 376

[4] Youssry I *et al* 2009 Skin iron concentration: a simple, highly sensitive method for iron stores evaluation in thalassemia patients *Hemoglobin* **31** 357–65

[5] Agarwal S and Krishnamurthy K 2019 Histology, skin *StatPearls* (StatPearls Publishing) (http://europepmc.org/books/NBK537325)

[6] Desouza E D *et al* 2013 Characterization of the depth distribution of Ca, Fe and Zn in skin samples, using synchrotron micro-x-ray fluorescence (SμXRF) to help quantify in-vivo measurements of elements in the skin *Appl. Radiat. Isot.* **77** 68–75

[7] Guinote I *et al* 2006 Using skin to assess iron accumulation in human metabolic disorders *Nucl. Instruments Methods Phys. Res.*B **249** 697–701

[8] Summerfield A, Meurens F and Ricklin M E 2015 The immunology of the porcine skin and its value as a model for human skin *Mol. Immunol.* **66** 14–21

[9] Meurens F, Summerfield A, Nauwynck H, Saif L and Gerdts V 2012 The pig: a model for human infectious diseases *Trends Microbiol.* **20** 50–7

[10] Liu Y *et al* 1936 Light microscopic, electron microscopic, and immunohistochemical comparison of bama minipig (Sus scrofa domestica) and human skin *Radiology* **27** 651–5

[11] Barbero A M and Frasch H F 2009 Pig and guinea pig skin as surrogates for human *in vitro* penetration studies: a quantitative review *Toxicol. Vitr.* **23** 1–13

[12] Nuttall K L, Gordon I H, Ow K and Ash E N 1995 Inductively coupled plasma mass spectrometry for trace elem ent analysis in the clinical laboratory *Annals of Clinical & Laboratory Sciences* **25** 264–71

[13] Agilent 2024 Elemental analysis by ICP-MS, ICP-MS for metal analysis, ICP-MS vs ICP-QQQ (https://agilent.com/en/product/atomic-spectroscopy/elemental-analysis-by-icp-ms)

[14] Sachs A, Levine V E, Hill F C and Hughes R 1943 Copper and iron in human blood *Arch. Intern. Med.* **71** 489–501

[15] Pinheiro T *et al* 2014 Distribution and quantitation of skin iron in primary haemochromatosis: correlation with total body iron stores in patients undergoing phlebotomy *Acta Derm. Venereol.* **94** 14–9

[16] Pinheiro T, Silva J N, Alves L C and Filipe P 2003 Iron deposition in skin of patients with haemochromatosis *Nucl. Instruments Methods Phys. Res.* B **210** 373–7

[17] Pinheiro T *et al* 2009 Imaging iron in skin and liver: Non-invasive tools for hemochromatosis therapy *Nucl. Instruments Methods Phys. Res.*B **267** 2140–3

[18] Oltulu P, Ince B, Kökbudak N, Findik S and Kiliç F 2018 Measurement of epidermis, dermis, and total skin thicknesses from six different body regions with a new ethical histometric technique, *Turkish J. Plast. Surg.* **26** 56–61